Short-range, overpressure-driven methane migration in coarse-grained gas hydrate reservoirs

Michael Nole[1], Hugh Daigle[1], Ann E. Cook[2], and Alberto Malinverno[3]

[1]Department of Petroleum and Geosystems Engineering, University of Texas at Austin, Austin, TX, USA

[2]School of Earth Sciences, The Ohio State University, Columbus, OH, USA

[3]Lamont Doherty Earth Observatory of Columbia University, Palisades, NY, USA

Corresponding author: Michael Nole (michael.nole@utexas.edu)

Key Points:

- Short-range advection is proposed as a methane migration mechanism in marine hydrate-bearing sands.
- Hydrate distributions in overpressured coarse-grained sands are hypothesized as functions of sand dip angle.
- 2D basin-scale simulations show overpressured flow focusing as a significant means of methane transport in sands.

Abstract

Two methane migration mechanisms have been proposed for coarse-grained gas hydrate reservoirs: short-range diffusive gas migration and long-range advective fluid transport from depth. Herein we demonstrate that short-range fluid flow due to overpressure in marine sediments is a significant additional methane transport mechanism that allows hydrate to precipitate in large quantities in thick, coarse-grained hydrate reservoirs. Two-dimensional simulations demonstrate that this migration mechanism, short-range advective transport, can supply significant amounts of dissolved gas and is unencumbered by limitations of the other two end-member mechanisms. Short-range advective migration can increase the amount of methane delivered to sands as compared to the slow process of diffusion, yet it is not necessarily limited by effective porosity reduction as is typical of updip advection from a deep source.

1 Introduction

An ice-like compound of natural gas molecules trapped in water lattices [*Sloan and Koh*, 2007], gas hydrate commonly forms within sediments along marine continental margins and under arctic permafrost [*Paull and Dillon*, 2001]. Natural sub-seafloor gas hydrate accumulations have been studied around the globe through a variety of subsurface, downhole, and laboratory techniques. Attention in recent years has focused on the northern Gulf of Mexico [*Boswell et al.*, 2009], the Nankai Trough off the southeast coast of Japan [*Uchida et al.*, 2004; *Fuji et al.*, 2008], the Krishna-Godavari Basin offshore India [*Collett* et al., 2008; *Ramana, et al.*, 2008; *Lee and Collett,* 2009], the northern Cascadia margin offshore the western U.S. and Canada [*Suess et al.*, 2001; *Riedel et al.*, 2006], the Ulleung Basin in the East Sea [*Kim et al.*, 2011], the South China Sea [*Wu et al.*, 2005], and Blake Ridge off the coast of the Carolinas [*Holbrook et al.*, 1996; *Collett and Ladd*, 2000]. These studies make use of well logs and 2D/3D

seismic data to interpret occurrences of gas hydrate and hypothesize mechanisms behind how hydrate accumulations can be expected to vary across heterogeneous lithologies. Accumulations of gas hydrate in nature are understood to represent a large global reservoir of methane gas and are thus important as a potential source of energy and/or greenhouse gas emissions, yet their formation and distribution remain somewhat enigmatic.

Observations of *in-situ* gas hydrate accumulations in marine sediments have illustrated vast heterogeneity in hydrate location and distribution in natural environments. In such areas as Walker Ridge in the northern Gulf of Mexico [*Frye et al.*, 2012] and the northern Cascadia margin offshore Canada [*Torres et al.*, 2008], large saturations of gas hydrate (upward of 50%) are observed to accumulate in coarse-grained sands (ranging in thickness from tens of centimeters to several meters) surrounded by fine-grained sediments containing little or no hydrate [*Cook and Malinverno*, 2013; *Malinverno,* 2010].

To explain the occurrence of massive gas hydrate accumulations in coarse-grained sand bodies bounded by hydrate-free fine-grained sediments, two end-member methane gas migration mechanisms have been invoked. The first, long-range advective migration, requires either a free gas source or a deep fluid source rich in methane to be sufficiently pressurized to drive fluid updip along a high permeability sand. Once these fluids reach the gas hydrate stability zone (GHSZ), concentrated hydrate deposits can precipitate directly from a gas phase migrating through the GHSZ [*Haeckel et al.*, 2004], or dissolved methane can drop out of aqueous solution as solid hydrate due to a reduction in solubility. This mechanism has been proposed mainly where a deeper thermogenic gas source or relatively deep (beneath the GHSZ) microbially-generated source is suspected, such as the Gulf of Mexico [*Boswell et al.*, 2012], offshore Brunei [*Warren et al.*, 2010], or the Hikurangi subduction margin offshore New Zealand [*Kroeger et al.*,

2015]. The difficulties with successfully invoking this mechanism to explain high hydrate saturations in sands include: (1) hydrate growth reduces effective porosity, which drops permeability and makes it difficult to preferentially channel pressurized fluid updip along a sand body; (2) methane hydrate growth is limited by the change in methane solubility in the sand with depth; and (3) a sand layer within the hydrate stability zone must be hydraulically connected to a deep methane source, which can be located at long distances down dip, creating particular difficulty for supplying methane to shallow sands.

Alternatively, short-range diffusive migration transports methane generated microbially within fine-grained clays in the hydrate stability zone into nearby sands along a persistent concentration gradient created by a higher effective methane solubility in the fine-grained sediments [*Clennel et al.*, 1999; Liu and Flemings, 2011; Rempel, 2011]. This migration mechanism has been invoked to describe gas hydrate accumulations offshore Canada [*Malinverno*, 2010]; in the northern Gulf of Mexico [*Cook and Malinverno*, 2013]; in the Andaman Sea, Indian Ocean; and the Kumano forearc basin, Nankai Trough offshore Japan [*Malinverno and Goldberg*, 2015]. In this scenario, effective porosity is reduced with hydrate growth as with a long-range advective mechanism, but methane transport occurs across a greater surface area of a sand body. While this mechanism allows for methane hydrate to accumulate on a regional scale throughout the hydrate stability zone without requiring a deep methane source, it may not be sufficient to explain high-saturation hydrate accumulations in thick sand layers.

We propose a new migration mechanism, short-range advective transport, which combines features of the two migration mechanisms above to explain the occurrence of high hydrate saturations in sand layers. Short-range advective transport occurs when a coarse-grained sand body is surrounded by overpressured fine-grained sediment. Methane enters a sand layer

entirely from within the GHSZ (short-range), yet the dominant transport mechanism is advection rather than diffusion. If the sand is dipping, far-field upward fluid flow within the surrounding low permeability, fine-grained material is diverted toward the base and downdip sides of the high permeability sand, which then channels fluid at high flow rates updip and expels it higher up in the bounding fine-grained sediment [*Flemings et al.*, 2002; *Berndt et al.*, 2005]. Limitations of updip advective transport are mitigated by providing a greater surface area over which methane can enter a sand within the GHSZ, and flow focusing can generate large updip flow velocities within the sand itself. The dissolved methane present in this type of system could be supplied by microbial methanogenesis within the hydrate stability zone, methane built up as free gas beneath the hydrate stability zone, or a deeper microbial or thermogenic source.

Free gas build-up upon hydrate dissociation with burial can generate overpressuring in hydrate systems, because a low-density gas column blocked from flowing upward can maintain a higher pressure than overlying water [*Hornbach et al.*, 2004]. Since this mechanism provides both a source of overpressuring and a source of methane, it could be effective in both focusing flow into dipping sands and recycling methane back into sands as solid hydrate. Both the sand-clay methane solubility contrast as well as the updip fluid flow velocity would contribute to the amount of methane that can be transported through overpressured flow focusing. Although hydrate growth still reduces effective porosity (and thus permeability), in this type of system methane transport into the sand occurs across a greater surface area than a downdip advective mechanism, and the flow rate within the sand layer itself is enhanced by sand-clay permeability contrasts.

While permeability contrasts in hydrate systems have been shown to focus gas hydrate growth in sand layers [*Chatterjee et al.*, 2014]; the combined effects of pore size contrasts,

focused fluid flow, and sand layer burial through the GHSZ on gas hydrate growth in coarse-grained sands have not been fully explored. In this study, we employ 2D basin-scale reactive transport simulations to better understand the impact of focused fluid flow on both the relative quantity and spatial distribution of gas hydrate in marine sediments. We find that a short-range advective system can produce significant amounts of methane as hydrate in thick sand strata with hydrate-free zones in the wake of exiting fluid, resembling hydrate occurrences observed in nature.

2 Hydrate Formation and Distribution Potential due to Flow Focusing

We hypothesize that the quantity and distribution of gas hydrate in a sand body in an overpressured system primarily depends on the magnitude of overpressuring beneath a sand body, the dip angle of the sand, the difference in methane solubility between the sand and surrounding clay (which is a function of depth as well as pore size contrast), and the sand-clay permeability contrast. **Figure 1** contains a set of hypothetical fluid flow pathways in the vicinity of a sand body filling with hydrate for varying sand dip angles. Because flow in the vicinity of a sand body behaves differently depending on the sand's angle of inclination, the distribution of hydrate within a sand layer should correspondingly depend on the dip of the sand.

As illustrated in **Figure 1a**, we hypothesize that a horizontal sand will capture overpressured fluid along its base. As hydrate grows along the bottom of the sand, over time the permeability of the sand will drop and the fluid flux into the sand will decrease. Very little hydrate is able to grow above the base of the sand because the solubility contrast is small between the sand's base and its top; dissolved methane entering from below will tend to form

hydrate immediately upon entering the base of the sand layer. A dipping sand body, however, focuses fluid flow such that flow enters the sand from below and from the sides, before being channeled updip at a higher velocity and out into the surrounding clay [*Flemings et al*., 2002; *Berndt et al.*, 2005] (**Figure 1b**). As hydrate formation decreases the permeability of the sand, the flow shifts its focus updip, allowing flow to enter the sand at shallower depths. Methane-charged fluid can thus enter the sand not only at the deepest part of the sand, but also updip; hydrate growth blocks pore space downdip and only works to divert flow, focusing it farther updip. Over time, a sand body with greater dip should therefore be able to fill with greater amounts of hydrate. In the limit of a completely vertical sand body (**Figure 1c**), all flow driven from the clay, characterized by the far field flow velocity (u_{ff}), is captured within the sand over a distance away from the sand equal to the sand's length [*Phillips*, 1991].

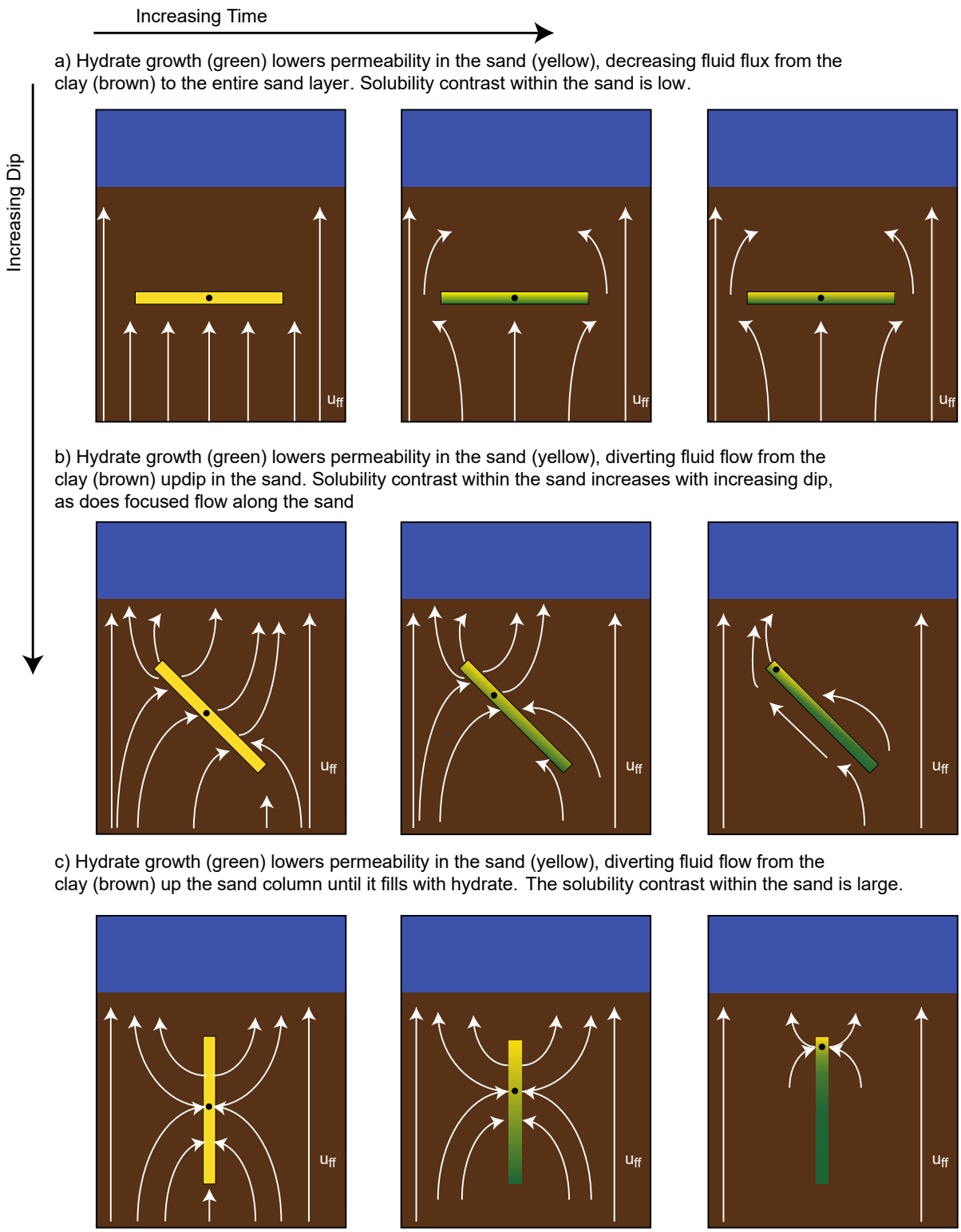
Increasing Time
Increasing Dip
a) Hydrate growth (green) lowers permeability in the sand (yellow), decreasing fluid flux from the clay (brown) to the entire sand layer. Solubility contrast within the sand is low.
u_{ff}
b) Hydrate growth (green) lowers permeability in the sand (yellow), diverting fluid flow from the clay (brown) updip in the sand. Solubility contrast within the sand increases with increasing dip, as does focused flow along the sand
u_{ff}
c) Hydrate growth (green) lowers permeability in the sand (yellow), diverting fluid flow from the clay (brown) up the sand column until it fills with hydrate. The solubility contrast within the sand is large.
u_{ff}

Figure 1. Diagram of the theoretical flow pattern of an overpressured system in which gas hydrate precipitates from methane-charged water. **a)** Flow lines diverge from a horizontal sand as hydrate accumulates at its base, **b)** flow lines focus updip in the sand as hydrate accumulates along its base and in its center, and **c)** as hydrate fills the sand from both sides and up its center, flow focuses updip. Flow into the sand is proportional to the length of the sand body divided by its width multiplied by the far field velocity, u_{ff}.

3 Simulation Methods

To test our hypothesis that a dipping sand body exposed to overpressured, methane-charged fluid in the gas hydrate stability zone will focus flow updip and fill with hydrate, we employ a basin-scale gas hydrate reservoir simulator. The simulations performed in this work bury a dipping, tabular sand body encased in low-permeability marine mud through the GHSZ. That is, the sand layer moves progressively deeper into the GHSZ with time as younger sediment layers are deposited on top of it. Methane is produced within the clays through microbial activity in the shallow sediment column, and overpressured fluids inject methane-charged water into the base of the hydrate stability zone at an aqueous methane concentration equal to the solubility of methane just above the base of the model (characteristic of a system where buried hydrate dissociates beneath the base of the gas hydrate stability zone) [*Bhatnagar et al.*, 2007].

Methane hydrate growth is tracked in 2D by solving a system of highly coupled, nonlinear mass balance equations for methane and water along with a system energy balance. Using a finite volume difference method, the solution scheme employs primary variable switching and iterates on nonlinearities using a Newton-Raphson search method. The numerical model is described in detail in *Sun and Mohanty* [2005]. The governing equations as well as the flow and heat transfer models are summarized in the Supplementary Information. Below, we

discuss the processes incorporated in the simulator that exert significant influence on hydrate accumulation due to flow focusing in heterogeneous systems.

3.1 Microbial Methanogenesis

Microbial methane sourcing is expressed as a steady-state exponentially decaying function of depth according to the formulation of *Malinverno* [2010]:

$$\boldsymbol{q(z) = k_{\alpha}\lambda\alpha_{SMT}\exp[-\frac{\lambda}{\omega}(z - z_{SMT})]}, \qquad (1)$$

where *q(z)* is the depth-varying methane source term to the clay grid blocks in the model, k_{α} is a conversion factor from metabolizable organic matter to methane (2241 kg/m^3 [*Malinverno,* 2010], λ is the metabolic reaction rate of microbial methanogenesis, α_{SMT} is the total amount of metabolizable organic carbon at the base of the sulfate reduction zone (the sulfate-methane transition), ω is the sedimentation rate, and z_{SMT} is the depth below seafloor of the sulfate-methane transition.

3.2 The Gibbs-Thomson Effect

The pore size contrast between clays and sands means that the effective methane solubility is higher in clays than sands. This difference results in a dissolved methane concentration gradient at the sand-clay contact that can drive diffusive methane flux from clays to sands and can also allow for advective methane transport within the clays at dissolved methane concentrations above the solubility of the sands. Known as the Gibbs-Thomson effect, an increase in curvature with decreasing pore size in a porous medium causes the solid-liquid interfacial energy of a crystal precipitating from the dissolved phase to increase the overall Gibbs free energy of the system. In a system of dissolved

gas and water, this in turn leads to an increase in the effective solubility of methane in smaller pores, inhibiting hydrate growth in comparison to bulk water [*Clennell et al.*, 1999]. This phenomenon is implemented in the simulator as a depression in the methane hydrate freezing temperature as follows [*Anderson et al.*, 2009]:

$$\Delta \boldsymbol{T_m} = \frac{-\boldsymbol{T_{mb}} * \boldsymbol{2} * \boldsymbol{\sigma_{hl}} * \cos(\boldsymbol{\theta})}{\boldsymbol{H_f} * \boldsymbol{\rho_h} * \boldsymbol{r}}, \qquad (2)$$

where T_{mb} is the bulk melting temperature of methane hydrate, σ_{hl} is the solid-liquid interfacial energy between hydrate and liquid water, set at 0.027 N/m [*Clennell et al.*, 1999], $\boldsymbol{\theta}$ is the hydrate wetting angle (0° assuming hydrate is a nonwetting phase), H_f, the hydrate bulk enthalpy of fusion, is 439 kJ/kg, ρ_h is the density of methane hydrate, 925 kg/m^3 [*Waite et al.*, 2009], and r is the pore radius governing effective methane solubility.

In the current work, we neglect pore size distribution and pore curvature impacts on the Gibbs-Thomson equation, which would reformulate effective methane solubility additionally as a function of hydrate saturation [*Liu and Flemings,* 2011; *Rempel*, 2011]. In terms of Equation (2), an increase in hydrate saturation would decrease the effective pore radius, intensify the freezing point depression, and increase the methane solubility. While this would limit the rate of change of hydrate saturation within a sand layer at small grid spacing and high hydrate saturation, the focus of this work is on the first order effects of fluid flow and permeability reduction on gas hydrate accumulations in a dipping sand at a relatively coarse spatial resolution.

3.3 Sedimentation and Burial

Over geologic time in marine basins, sedimentation works to consolidate and bury material once deposited at the seafloor. Additionally, tectonic activity can deform sediments while they are buried. The stratigraphic relationships between sediments of varying lithologies can potentially have a large impact on basin-scale fluid flow and methane transport, so it is essential to capture stratigraphic evolution in 2D and 3D basin-scale models. In order to incorporate sedimentation effects over geologic time on the spatial evolution of different lithologic units from horizontal and flat to dipping and curved, this simulator expresses lithologic properties as functions of both space and time.

Sediment porosity is expressed as an exponentially decaying function of depth [*Rubey and Hubbert*, 1959]:

$$\boldsymbol{\phi} = \boldsymbol{\phi}_{\infty} + (\boldsymbol{\phi_0} - \boldsymbol{\phi}_{\infty})\boldsymbol{e}^{-\left(\frac{\sigma_e}{\sigma_\phi}\right)} \qquad (3)$$

where ϕ_0 is the sediment porosity at the seafloor (set at 75%), ϕ_∞ is the asymptotic porosity achieved (set at 30%), σ_e is the effective stress (lithostatic stress less pore pressure), and σ_ϕ is a characteristic stress constant, set at 20 MPa.

Permeability evolves as sediments are compacted with burial according to a Kozeny-Carman permeability-porosity power law relationship [*Civan*, 2001]:

$$\boldsymbol{k} = \frac{\boldsymbol{\phi k_0}}{\boldsymbol{\phi_0}}\left(\frac{\boldsymbol{\phi(1-\phi_o)}}{\boldsymbol{\phi_o(1-\phi)}}\right)^{\boldsymbol{2\beta}} \qquad (4)$$

where β, the power law parameter, is set to 2 (see *Sun and Mohanty* [2006]), and k_0 is a reference seafloor permeability (set to 1 Darcy [10^{-12} m^2] in the clay).

Additionally, permeability decreases with increasing saturation of pore-filling hydrate as follows [*Dai and Seol*, 2014]:

$$\boldsymbol{k'} = \boldsymbol{k}\frac{(1-S_h)^3}{(1+2S_h)^2} \qquad (5)$$

where *k'* is the sediment permeability in the presence of hydrate, *k* is the clean sediment permeability in the absence of hydrate, and S_h is the hydrate saturation.

4 Results and Discussion

Walker Ridge in the northern Gulf of Mexico has been identified as a significant gas hydrate prospect and is the subject of upcoming exploratory drilling expeditions; observed hydrate accumulations in sands both shallow and deep indicate that multiple methane migration mechanisms could be contributing to hydrate accumulations in this region. Therefore, the environmental parameters used in this study were selected to emulate a Walker Ridge-like gas hydrate system in which a deep seafloor (set to 1917 m) and a low local geothermal gradient (19.6 ^{o}C/km) contribute to a thick hydrate stability zone (approximately 900 m thick) [*Collett et al.*, 2012] that is microbially active and potentially subject to overpressuring at depth. Parameters describing the rate of microbial methanogenesis are not well constrained at Walker Ridge; α_{SMT} is approximated as 0.5 dry wt% (following *Malinverno*, [2010]), λ is set at $1x10^{-12}$ per second, ω is approximately 1 mm/yr [*Boswell et al.*, 2012], and z_{SMT} is estimated as 10 m [Kastner et al., 2008; Smith et al., 2014]. An overpressured system is simulated in this study by imposing a hydrostatic pressure boundary condition at the seafloor (the top of the model domain), no flow boundaries on the sides of the domain, and a constant pressure boundary condition at the base of the gas hydrate stability zone (BHSZ). The overpressure boundary condition was estimated for

this environment using a 10.5 ppg mud weight [*Collett et al.*, 2012]; since the weight of seawater is approximately 8.6 ppg (at a density of 1030kg/m^3), overpressured fluid at the BHSZ is set at 1.22 times the hydrostatic pressure.

A binary system of sand and clay lithologies is considered. To isolate the majority of hydrate growth to the sand layer from the rest of the domain, the sand lithology is characterized by pore radii of 10 microns, in which methane solubility is nearly the same as that of bulk seawater, and the clay pore size is modeled as 10 nanometers (an approximate median pore size as indicated by NMR log data at nearby Keathley Canyon in the Gulf of Mexico [*Bihani et al.*, 2015]), at which point effective aqueous methane solubility is enhanced to inhibit hydrate growth outside the sand. Within the simulation domain, a 36.6 m thick section of grid blocks labeled as sand lithology are initially oriented horizontally, with a length of 2.3 km. Each sand grid block moves down through the domain with a particular sedimentation velocity; this velocity varies spatially to allow rotation until reaching the midpoint of the domain, at which point the dip of the sand body is held constant at 10 degrees while it is buried to the bottom of the domain. The surrounding clays are initialized with 6 orders of magnitude lower permeability than the sand. The initial permeability values are set according to the permeability-porosity relationship described above.

Figure 2 illustrates a 2D view of the planar sand body modeled in this work: it is first deposited flat and then rotates to dip as depicted in the diagram. A pressure profile depicts the hydrostatic and approximate lithostatic pressure gradients along with a transect mapping the pressure through the sand after it is buried in an overpressured clay to just above the BHSZ. For this comparison, lithostatic stress was approximated assuming a clay grain density of 2800 kg/m^3. Because the permeability in the sand is so high, excess pressure is very quickly dissipated

as fluid flows updip. The pressure gradient in the sand is therefore lower than that in the surrounding clays, approaching the hydrostatic gradient, as is often observed in natural overpressured environments [*Flemings et al.*, 2002].

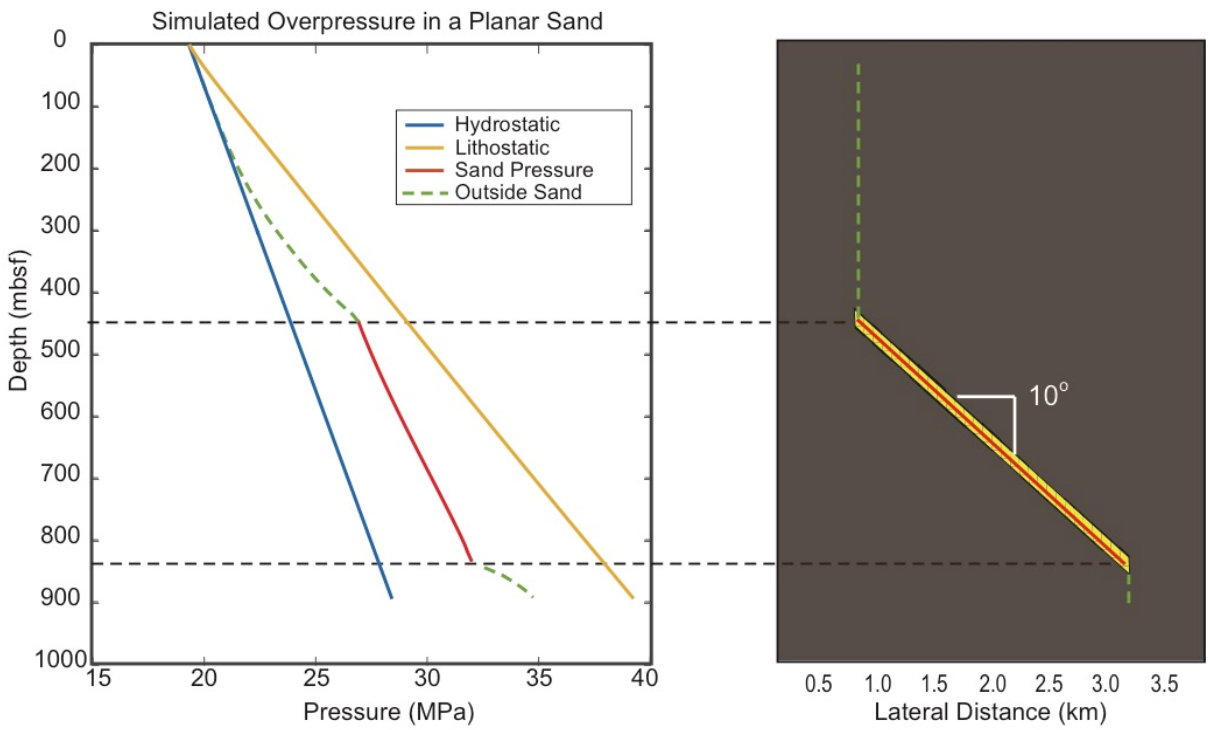

Figure 2. Simulated pressure profile through a buried dipping sand (left), along with a physical depiction of the simulated sand (right). The sand body in this simulation is dipping at 10 degrees, and its thickness is 36.6 m.

Two-dimensional simulation profiles depicted in **Figure 3** illustrate the regional-scale impact of methane-charged, focused fluid flow within the GHSZ. Hydrate growth (**Figure 3a**) is restricted mainly to the sand body; it is concentrated unevenly down dip and along the base of the gently dipping sand, and minimal hydrate saturations are present in the clay because of focused methane transport. The permeability of the sand drops correspondingly, mirroring what

would be anticipated based on the expected flow focusing pattern in the dipping sand diagram shown in **Figure 1b**.

Methane solubility increases with depth in the sediment column, shown in the aqueous methane concentration profile (**Figure 3c**). Throughout the domain away from the sand, fluid flux is sufficiently low that only very small hydrate saturations exist and pore water methane concentrations are equal to the solubility of methane (contours are horizontal and parallel). Directly above the sand, aqueous methane concentrations are undersaturated with respect to the solubility of the clays because net fluid migration is out of the sand, carrying fluid with a dissolved methane concentration equal to the aqueous methane solubility of the sand. This creates a hydrate free zone in the wake of fluid exiting any dipping, overpressured sand. Very low hydrate saturations beneath the sand indicate fluid flow rates near the sand are high enough in this instance to precipitate hydrate accumulations that persist with burial.

The overpressure profile depicted in **Figure 3b** is indicative of the flow focusing that occurs in response to overpressure imposed on the bottom boundary of the system. Fluid streamlines flow perpendicular to pressure contours, so it is clear that if flow is being driven from the bottom of the domain, it will first flow toward the dipping sand and then become diverted updip before being expelled upward out of the sand. As hydrate precipitates out of this flowing fluid, the pore space in the sand becomes occluded, and thus the permeability of the sand drops. The permeability within the hydrate-bearing sand (**Figure 3d**) is 2-3 orders of magnitude lower than the seafloor permeability, but it is still 4-5 orders of magnitude greater than the fine-grained sediment around it. This indicates that although hydrate generation is decreasing permeability, focused fluid flow can still take place because a permeability contrast still exists to focus overpressured flow.

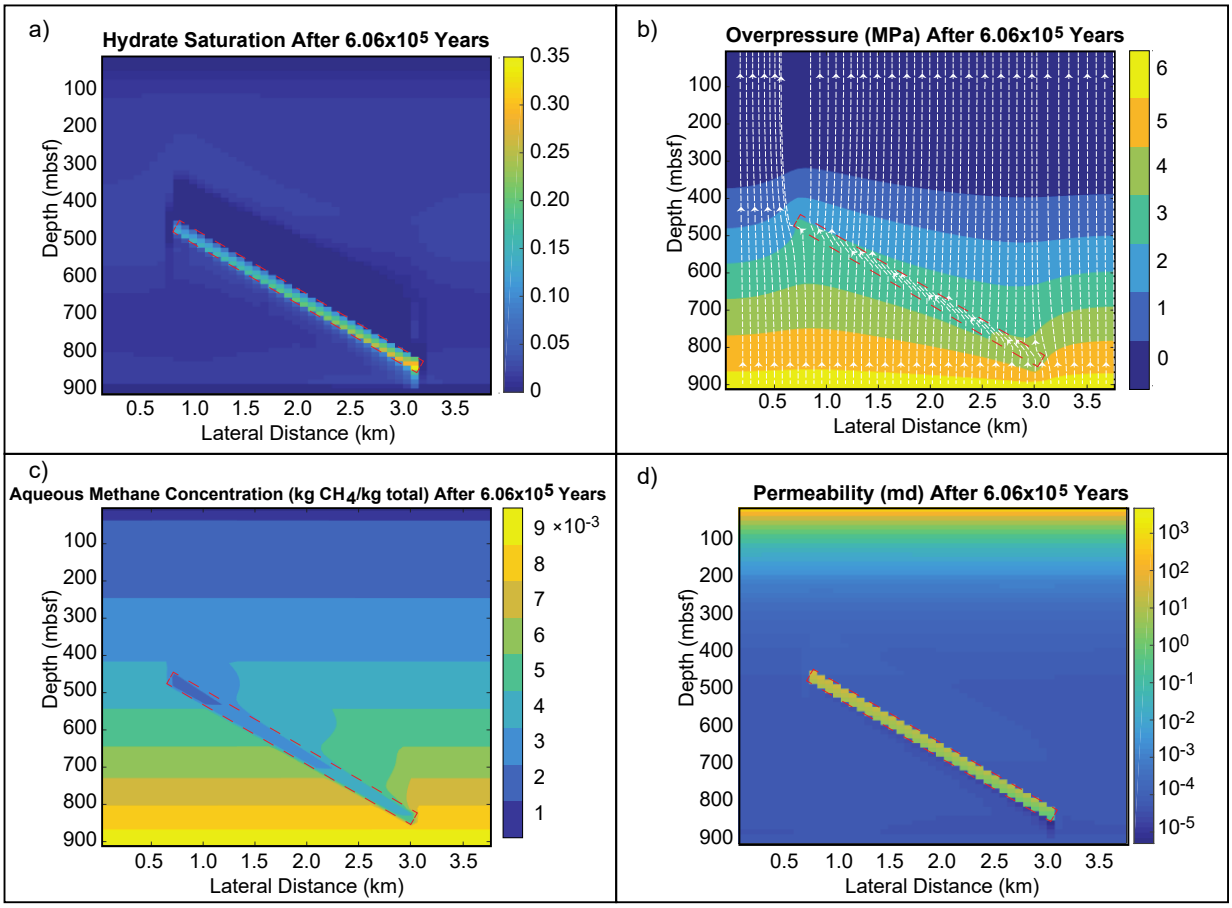

Figure 3. Profiles of hydrate saturation (**3a**), pore fluid overpressure (defined as the difference between fluid pressure and hydrostatic pressure) accompanied by fluid streamlines (white dashed lines) (**3b**), aqueous methane concentration (**3c**), and permeability (**3d**) in and around a dipping sand in an overpressured hydrate system located within the hydrate stability zone. The sand layer is outlined in red. The sand layer dips approximately 10 degrees from horizontal and is 36.6 m thick.

The results of these 2D simulations illustrate that overpressure-driven short-range advection within the GHSZ will focus methane-charged fluids into a dipping sand body, even under conditions of modest overpressuring (well below lithostatic pressure) and low dip angle. Correspondingly, hydrate growth reflects the fluid flow pattern, the sand-clay methane solubility contrast, and the methane solubility contrast within the sand itself. Even if the flow rate outside

of the sand is insufficient to produce much hydrate in the low permeability, fine-grained sediment, large amounts of hydrate can still precipitate in the sand because the sand-clay permeability contrast channels fluid updip at high velocity in a lithology where the effective methane solubility is lower and hydrate formation is favored. This stands in contrast to a diffusive system, where methane can only migrate along concentration gradients. For the simulated system described above, including the overpressuring boundary condition yields about 50% greater average hydrate saturations in the sand layer than simulating the environment as a diffusive system alone (see Supplementary Information).

As a hydrate-bearing sediments are buried beneath the GHSZ, overpressure produced via hydrate dissociation can be dissipated by channeling fluid into a sand layer from its sides instead of just downdip. This provides an effective mechanism for recycling methane back into sands as hydrate because fluids can enter the sand layer over greater surface area. If at any point the fluid pressure in an overpressured sand exceeds the minimum principal stress in the clay overburden, channeled fluid flow could induce fracturing in the bounding clay. In this instance, methane in the pore fluid could potentially precipitate out as hydrate within open fractures in clays, as the effective aqueous solubility of methane could be reduced to that of bulk seawater if fracture aperture is sufficiently wide.

5 Conclusions

We present short-range advective migration as a methane transport mechanism leading to methane hydrate accumulations in marine sands within the gas hydrate stability zone. Methane transport through fluid flow in the vicinity of a sand body is enhanced by both sand/clay solubility gradients and fluid flow within the sand. We hypothesize that when a high

permeability sand layer is enclosed in an overpressured, low permeability clay, the amount and distribution of gas hydrate within the sand will depend on its dip angle. Higher dip angles will tend to more strongly focus fluid flow into the sand, which over time will more evenly distribute gas hydrate throughout the sand layer. In order to validate this hypothesis, we utilized 2D basin-scale methane hydrate reservoir simulations. We show that by imposing an overpressuring lower boundary condition, methane-charged fluid flow is focused from a bounding clay updip along a thick dipping sand. Short-range advective migration mechanism combines the methane transport mechanisms of both short-range diffusive migration and long-range advective migration, in that it is magnified by large clay-sand spatial solubility gradients and significant updip fluid flow. As a methane supply mechanism to thick dipping sand bodies, it has the potential to transport significantly more methane faster than diffusive migration and with the benefit of not being restricted by sand pore blockage, as is typical of long-distance advective transport.

While this work demonstrates the impact overpressuring can have on hydrate formation on a dipping sand confined to within the gas hydrate stability zone, future work will elucidate the impact of short range advective methane transport on hydrate growth patterns in multilayered sand systems, building off of the approach of *Rempel,* 2011. Because fluid exiting a sand body from above is undersaturated in methane with respect to the solubility of the surrounding clay, it is likely that in a multilayered system high hydrate saturations in sand layers could be separated by hydrate free zones in clays between them. The mechanism proposed in this work could be applicable anywhere in the GHSZ where *in situ* pressure measurements indicate contrasts in pressure gradients between sands and clays, as **Figure 2** illustrates.

Acknowledgments

We would like to gratefully acknowledge Gareth Crutchley and an anonymous reviewer for providing constructive feedback, which greatly benefitted the clarity of this manuscript. Supporting data are included in an SI file; additional information may be obtained by request (michael.nole@utexas.edu).

This material is based upon work supported by the Department of Energy under Award Number DE-FE0013919. This report was prepared as an account of work sponsored by an agency of the United States Government. Neither the United States Government nor any agency thereof, nor any of their employees, makes any warranty, express or implied, or assumes any legal liability or responsibility for the accuracy, completeness, or usefulness of any information, apparatus, product, or process disclosed, or represents that its use would not infringe on privately owned rights. Reference herein to any specific commercial product, process, or service by trade name, trademark, manufacturer, or otherwise does not necessarily constitute or imply its endorsement, recommendation, or favoring by the United States Government or any agency thereof. The views and opinions of authors expressed herein to not necessarily state or reflect those of the United States Government or any agency thereof.

References

Anderson, R., Bahman Tohidi, and J. Beau W. Webber. "Gas hydrate growth and dissociation in narrow pore networks: capillary inhibition and hysteresis phenomena." Geological Society, London, Special Publications 319, no. 1 (2009): 145-159.

Berndt, C. (2005). Focused fluid flow in passive continental margins. Philosophical Transactions of the Royal Society of London A: Mathematical, Physical and Engineering Sciences, 363(1837), 2855-2871.

Bhatnagar, G., Chapman, W. G., Dickens, G. R., Dugan, B., and Hirasaki, G. J. (2007). Generalization of gas hydrate distribution and saturation in marine sediments by scaling of thermodynamic and transport processes. American Journal of Science, 307(6), 861-900.

Bihani, A., Daigle, H., Cook, A., Glosser, D., Shushtarian, A., Pore size distribution and methane equilibrium conditions at Walker Ridge Block 313, northern Gulf of Mexico, abstract OS23B-1999, American Geophysical Union Fall Meeting, San Francisco, CA, 15 December 2015.

Boswell, R., Collett, T., McConnell, D., Frye, M., Shedd, B., Mrozewski, S., Gilles Guerin, Ann Cook, Paul Godfriaux, Rebecca Dufrene, Rana Roy, and Emrys Jones (2009). Joint Industry Project Leg II discovers rich gas hydrate accumulations in sand reservoirs in the Gulf of Mexico. Natural Gas and Oil, 304, 285-4541.

Boswell, R., Frye, M., Shelander, D., Shedd, W., McConnell, D. R., and Cook, A. (2012). Architecture of gas-hydrate-bearing sands from Walker Ridge 313, Green canyon 955,

and Alaminos canyon 21: northern deepwater Gulf of Mexico. Marine and Petroleum Geology, 34(1), 134-149.

Chatterjee, S., Bhatnagar, G., Dugan, B., Dickens, G. R., Chapman, W. G., and Hirasaki, G. J. (2014). The impact of lithologic heterogeneity and focused fluid flow upon gas hydrate distribution in marine sediments. Journal of Geophysical Research: Solid Earth, 119(9), 6705-6732.

Civan, F. (2001). Scale effect on porosity and permeability: Kinetics, model, and correlation. AIChE journal, 47(2), 271-287.

Clennell, M. B., Hovland, M., Booth, J. S., Henry, P., and Winters, W. J. (1999). Formation of natural gas hydrates in marine sediments: 1. Conceptual model of gas hydrate growth conditioned by host sediment properties. Journal of Geophysical Research: Solid Earth, 104(B10), 22985-23003.

Collett, T. S., and Ladd, J. (2000). 19. Detection of gas hydrate with downhole logs and assessment of gas hydrate concentrations (saturations) and gas volumes on the Blake Ridge with electrical resistivity log data. In Proceedings of the Ocean Drilling Program. Scientific Results (Vol. 164, pp. 179-191). Ocean Drilling Program.

Collett, T. S., Lee, M. W., Zyrianova, M. V., Mrozewski, S. A., Guerin, G., Cook, A. E., and Goldberg, D. S. (2012). Gulf of Mexico Gas Hydrate Joint Industry Project Leg II logging-while-drilling data acquisition and analysis. Marine and Petroleum Geology, 34(1), 41-61.

Collett, T.S., Riedel, M., Cochran, J.R., Boswell, R., Kumar, P., Sathe, A.V., the NGHP Exp. 01 Scientific Party (2008). Indian continental margin gas hydrate prospects: results of the

Indian National Gas Hydrate program (NGHP) expedition 01. Proc. of the 6th International Conference on Gas Hydrates (ICGH 2008). Vancouver, BC, Canada.

Cook, A. E., and Malinverno, A. (2013). Short migration of methane into a gas hydrate-bearing sand layer at Walker Ridge, Gulf of Mexico. Geochemistry, Geophysics, Geosystems, 14(2), 283-291.

Dai, S., and Seol, Y. (2014). Water permeability in hydrate-bearing sediments: A pore-scale study. Geophysical Research Letters, 41(12), 4176-4184.

Flemings, P. B., Stump, B. B., Finkbeiner, T., and Zoback, M. (2002). Flow focusing in overpressured sandstones: Theory, observations, and applications. American Journal of Science, 302(10), 827-855.

Frye, M., Shedd, W., and Boswell, R. (2012). Gas hydrate resource potential in the Terrebonne Basin, Northern Gulf of Mexico. Marine and petroleum geology, 34(1), 150-168.

Fujii, T., Saeki, T., Kobayashi, T., Inamori, T., Hayashi, M., Takano, O., ... and Yokoi, K. (2008, January). Resource assessment of methane hydrate in the eastern Nankai Trough, Japan. In Offshore Technology Conference. Offshore Technology Conference.

Haeckel, M., Suess, E., Wallmann, K., and Rickert, D. (2004). Rising methane gas bubbles form massive hydrate layers at the seafloor. Geochimica et Cosmochimica Acta, 68(21), 4335-4345

Holbrook, W. S., Hoskins, H., Wood, W. T., Stephen, R. A., and Lizarralde, D. (1996). Methane hydrate and free gas on the Blake Ridge from vertical seismic profiling. Science, 273(5283), 1840.

Hubbert, M. K., and Rubey, W. W. (1959). Role of fluid pressure in mechanics of overthrust faulting I. Mechanics of fluid-filled porous solids and its application to overthrust faulting. Geological Society of America Bulletin, 70(2), 115-166.

Kastner, M., Claypool, G., and Robertson, G. (2008). Geochemical constraints on the origin of the pore fluids and gas hydrate distribution at Atwater Valley and Keathley Canyon, northern Gulf of Mexico. Marine and Petroleum Geology, 25(9), 860-872.

Kim, G. Y., Yi, B. Y., Yoo, D. G., Ryu, B. J., and Riedel, M. (2011). Evidence of gas hydrate from downhole logging data in the Ulleung Basin, East Sea. Marine and Petroleum Geology, 28(10), 1979-1985.

Kroeger, K. F., Plaza-Faverola, A., Barnes, P. M., and Pecher, I. A. (2015). Thermal evolution of the New Zealand Hikurangi subduction margin: impact on natural gas generation and methane hydrate formation–a model study. Marine and Petroleum Geology, 63, 97-114.

Lake, L.W. (1989). Enhanced Oil Recovery. Prentice-Hall Inc., Upper Saddle River, NJ.

Lee, M. W., and Collett, T. S. (2009). Gas hydrate saturations estimated from fractured reservoir at Site NGHP-01-10, Krishna-Godavari Basin, India. Journal of Geophysical Research: Solid Earth (1978–2012), 114(B7).

Liu, X., and Flemings, P. B. (2011). Capillary effects on hydrate stability in marine sediments. Journal of Geophysical Research: Solid Earth, 116(B7).

Malinverno, A. (2010) Marine gas hydrates in thin sand layers that soak up microbial methane, Earth and Planetary Science Letters 292, 399-408.

Malinverno, A., and Goldberg, D. S. (2015). Testing short-range migration of microbial methane as a hydrate formation mechanism: Results from Andaman Sea and Kumano Basin drill sites and global implications. Earth and Planetary Science Letters, 422, 105-114.

Paull, Charles K., and William P. Dillon. "Natural gas hydrates: occurrence, distribution, and detection." Washington DC American Geophysical Union Geophysical Monograph Series 124 (2001).

Phillips, O. M. (1991). Flow and reactions in permeable rocks. Cambridge University Press.

Ramana, M. V., Ramprasad, T., Paropkari, A. L., Borole, D. V., Rao, B. R., Karisiddaiah, M. Desa, M. Kocherla, H. M. Joao, P. Lokabharati, Maria-Judith Gonsalves, J. N. Pattan, N. H. Khadge, C. Prakash Babu, A. V. Sathe, P. Kumar, A. K. Sethi (2009). Multidisciplinary investigations exploring indicators of gas hydrate occurrence in the Krishna–Godavari Basin offshore, east coast of India. Geo-Marine Letters, 29(1), 25-38.

Rempel, A. W. (2011). A model for the diffusive growth of hydrate saturation anomalies in layered sediments. Journal of Geophysical Research: Solid Earth, 116(B10).

Riedel, M., T. S. Collett, M. J. Malone, and Expedition 311 Scientists (2006), Proceedings IODP, Exp. 311, Integrated Ocean Drilling Program Management International, Inc.

Sloan, E.D. and Koh, C.A. (2007). Clathrate hydrates of natural gases, third edition. 721 p. CRC Press, Boca Raton.

Smith, J. P., and Coffin, R. B. (2014). Methane Flux and Authigenic Carbonate in Shallow Sediments Overlying Methane Hydrate Bearing Strata in Alaminos Canyon, Gulf of Mexico. Energies, 7(9), 6118-6141.

Suess, E., Torres, M. E., Bohrmann, G., Collier, R., Rickert, D., Goldfinger, C., ... and Jung, C. (2001). Sea floor methane hydrates at Hydrate Ridge, Cascadia margin. Natural gas hydrates: occurrence, distribution, and detection, 87-98.

Sun, X., 2005. Modeling of hydrate formation and dissociation in porous media. Ph.D. Thesis, University of Houston, Houston, TX.

Sun, X., and Mohanty, K. K. (2006). Kinetic simulation of methane hydrate formation and dissociation in porous media. Chemical Engineering Science, 61(11), 3476-3495.

Torres, M.E., Tréhu, A.M., Cespedes, N., Kastner, M., Wortmann, U.G., Kim, J.-H., Long, P. E., Malinverno, A., Pohlman, J.W., Riedel, M., Collett, T.S., 2008. Methane hydrate formation in turbidite sediments of northern Cascadia, IODP Expedition 311. Earth Planet. Sci. Lett. 271, 170–180.

Uchida, T., Lu, H., and Tomaru, H. (2004). Subsurface occurrence of natural gas hydrate in the Nankai Trough area: Implication for gas hydrate concentration. Resource Geology, 54(1), 35-44.

Warren, J.K., Cheung, A., and Cartwright, I. (2010). Organic geochemical, isotopic, and seismic indicators of fluid flow in pressurized growth anticlines and mud volcanoes in modern deep-water slope and rise sediments of offshore Brunei Darussalam: Implications for hydrocarbon exploration in other mud- and salt-diapir provinces, *in* L. Wood, ed., Shale tectonics: AAPG Memoir 93, p. 163–196. doi:10.1306/13231314M933424

Wu, S. G., Zhang, G. X., Huang, Y. Y., Liang, J., and Wong, H. K. (2005). Gas hydrate occurrence on the continental slope of the northern South China Sea. Marine and Petroleum Geology, 22(3), 403-412.

Figure 1. Figure

Increasing Time

Increasing Dip

a) Hydrate growth (green) lowers permeability in the sand (yellow), decreasing fluid flux from the clay (brown) to the entire sand layer. Solubility contrast within the sand is low.

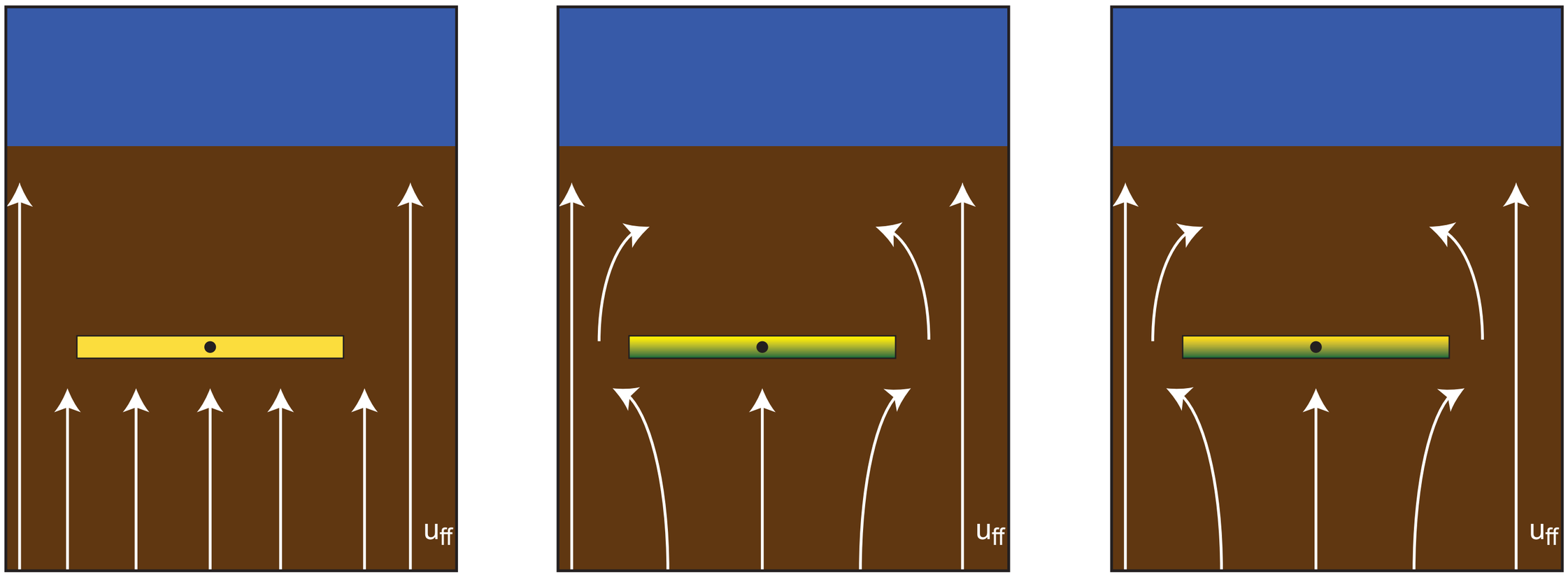

b) Hydrate growth (green) lowers permeability in the sand (yellow), diverting fluid flow from the clay (brown) updip in the sand. Solubility contrast within the sand increases with increasing dip, as does focused flow along the sand

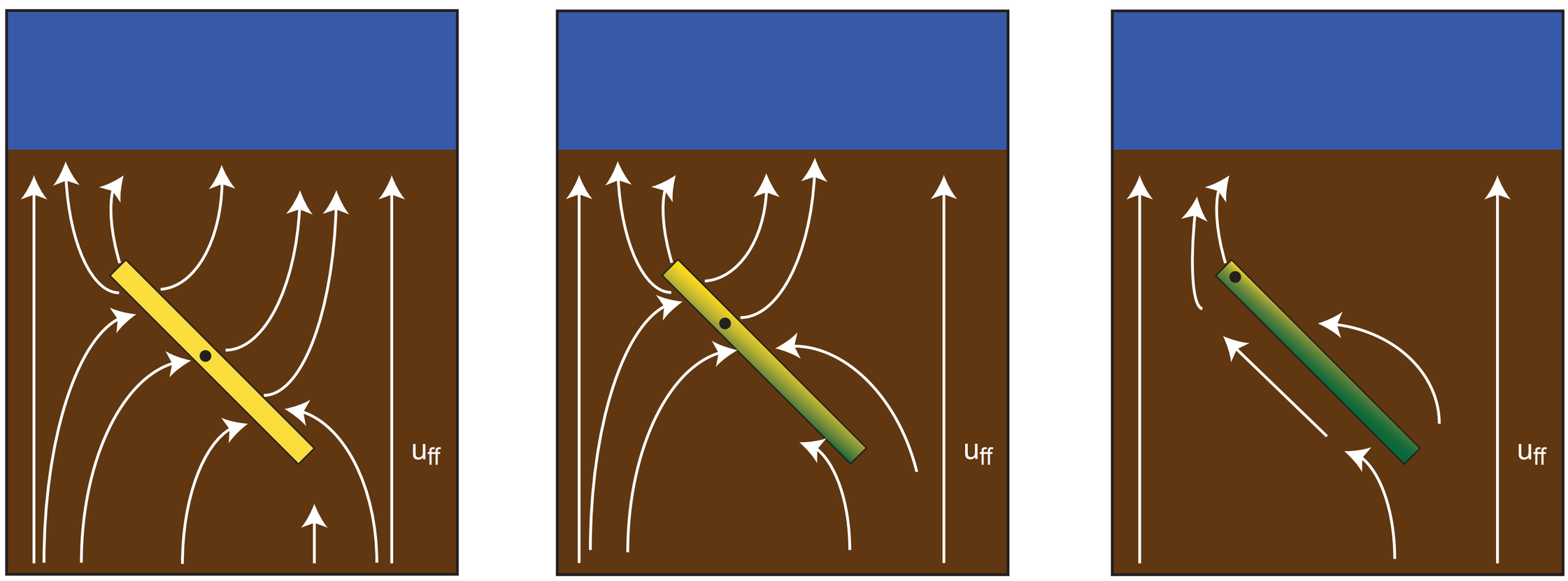

c) Hydrate growth (green) lowers permeability in the sand (yellow), diverting fluid flow from the clay (brown) up the sand column until it fills with hydrate. The solubility contrast within the sand is large.

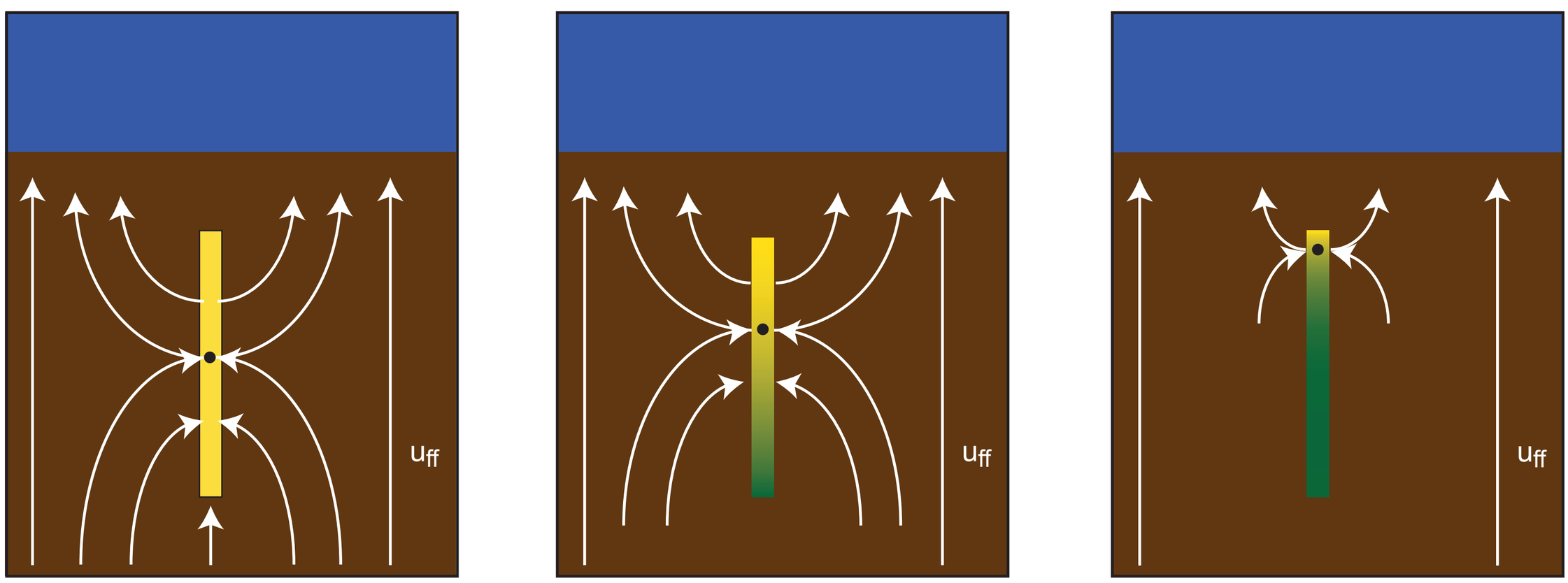

Figure 2. Figure

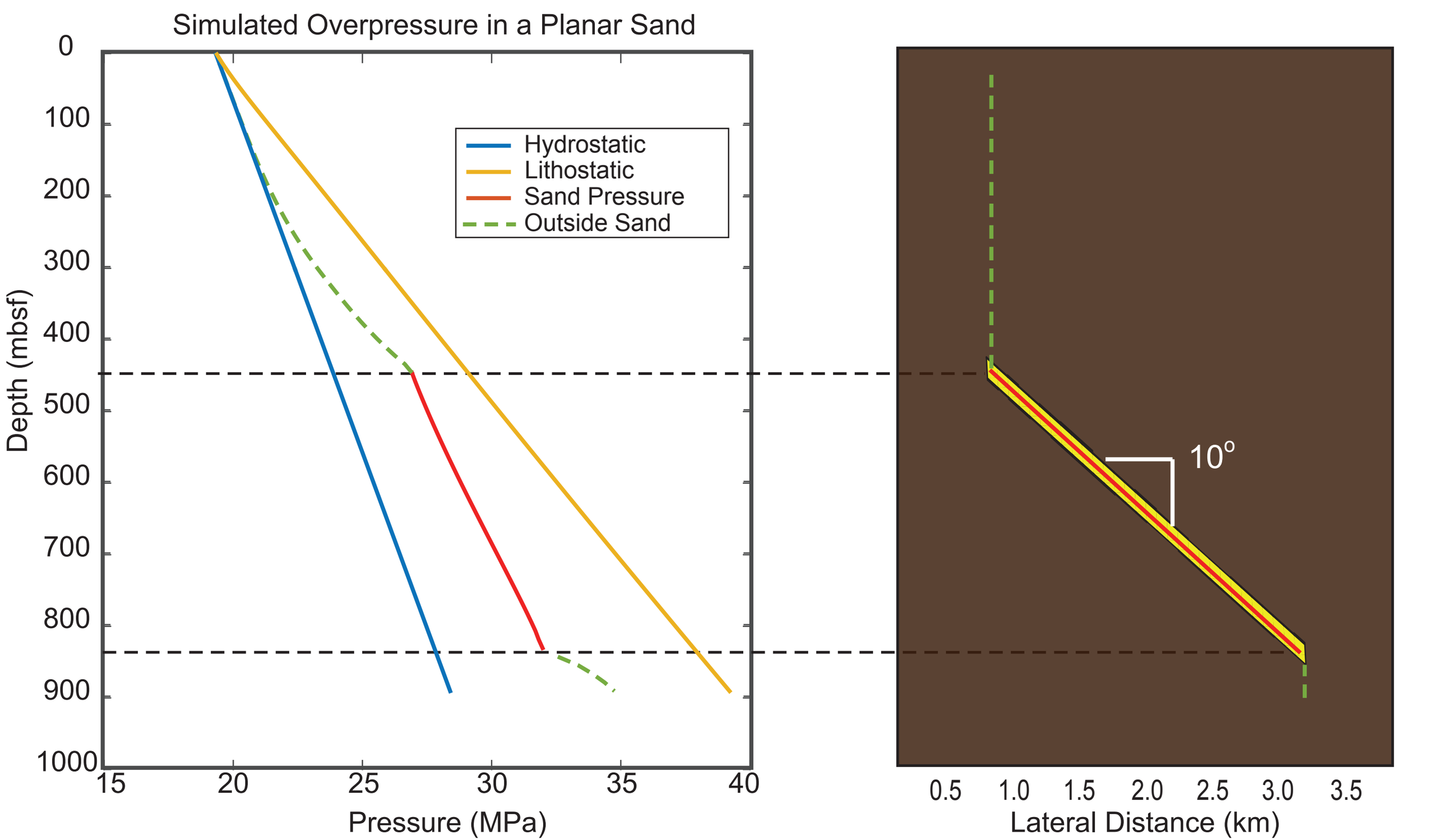
Simulated Overpressure in a Planar Sand
Hydrostatic
Lithostatic
Sand Pressure
Outside Sand
Depth (mbsf)
0
100
200
300
400
500
600
700
800
900
1000
15
20
25
30
35
40
Pressure (MPa)
10°
0.5
1.0
1.5
2.0
2.5
3.0
3.5
Lateral Distance (km)

Figure 3. Figure

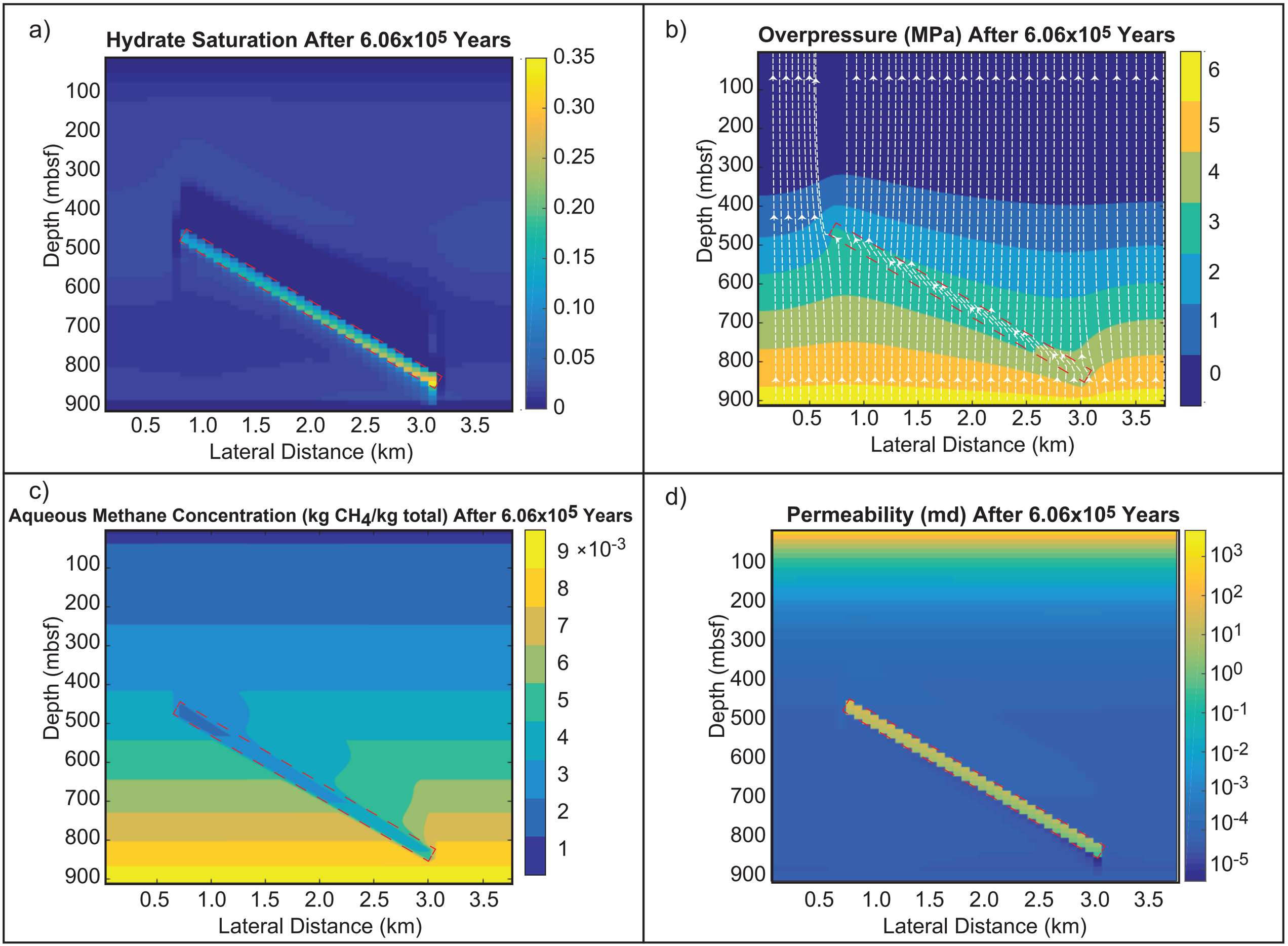
a)
Hydrate Saturation After 6.06x10^5 Years
Depth (mbsf)
Lateral Distance (km)
b)
Overpressure (MPa) After 6.06x10^5 Years
Depth (mbsf)
Lateral Distance (km)
c)
Aqueous Methane Concentration (kg CH4/kg total) After 6.06x10^5 Years
Depth (mbsf)
Lateral Distance (km)
d)
Permeability (md) After 6.06x10^5 Years
Depth (mbsf)
Lateral Distance (km)